Mechanistic Characterization of Aerobic Alcohol Oxidation Catalyzed by $Pd(OAc)_2$/Pyridine Including Identification of the Catalyst Resting State and the Origin of Non-Linear [Catalyst] Dependence

*Bradley A. Steinhoff, Ilia A. Guzei and Shannon S. Stahl**

Department of Chemistry, University of Wisconsin-Madison, 1101 University Avenue, Madison, WI 53706

Table of Contents **Pages**

O_2 dependence in the presence of 500 mM pyridine.

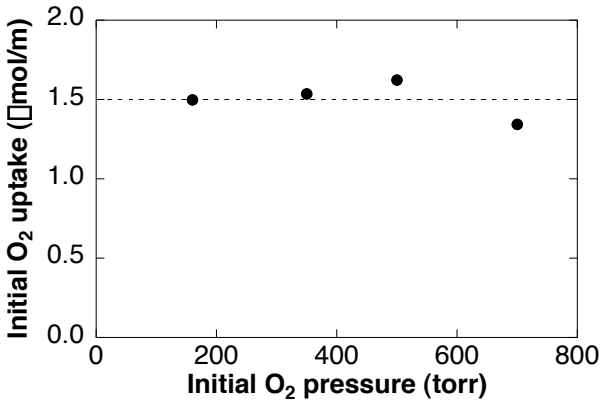

Figure S1. Dependence of the initial rate on the starting oxygen pressure with 500 mM pyridine. Conditions: [$Pd(OAc)_2$] = 5.0 mM, [pyridine] = 500 mM, [Alcohol] = 0.10 M, pO_2 = 160-700 torr, 80 °C.

NMR spectra of a titration of benzyl alcohol against $(py)_2Pd(OAc)_2$.

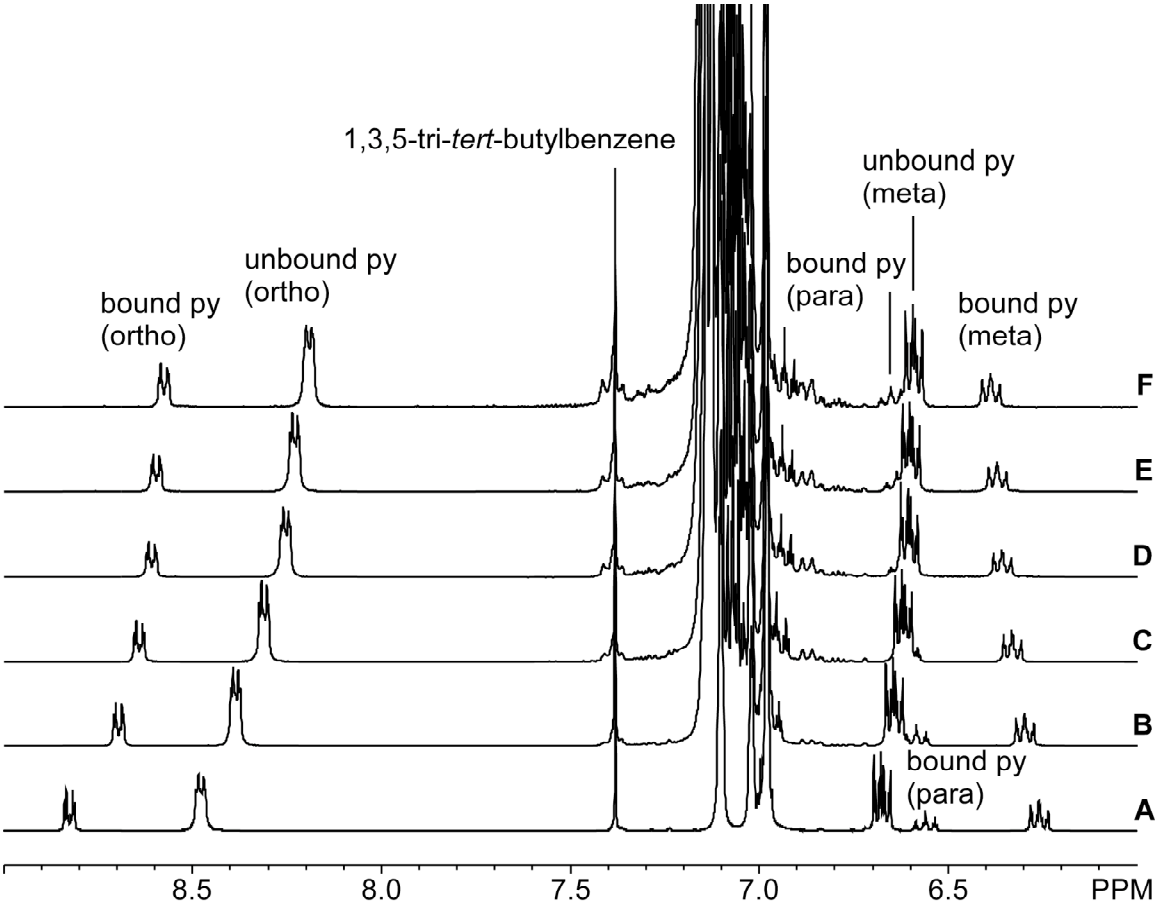

Figure S2. NMR spectra of a titration of benzyl alcohol against $(py)_2Pd(OAc)_2$. Conditions: $[Pd(OAc)_2]$ = 2.2 mM, [pyridine] = 15.1 mM, [alcohol] = 0-460 mM, [1,3,5-tri-*tert*-butylbenzene] = 3.1 mM, toluene-d_8, 22 °C. **A** = 0 M benzyl alcohol. **B** = 0.07 M benzyl alcohol. **C** = 0.18 M benzyl alcohol. **D** = 0.27 M benzyl alcohol. **E** = 0.35 M benzyl alcohol. **F** = 0.46 M benzyl alcohol.

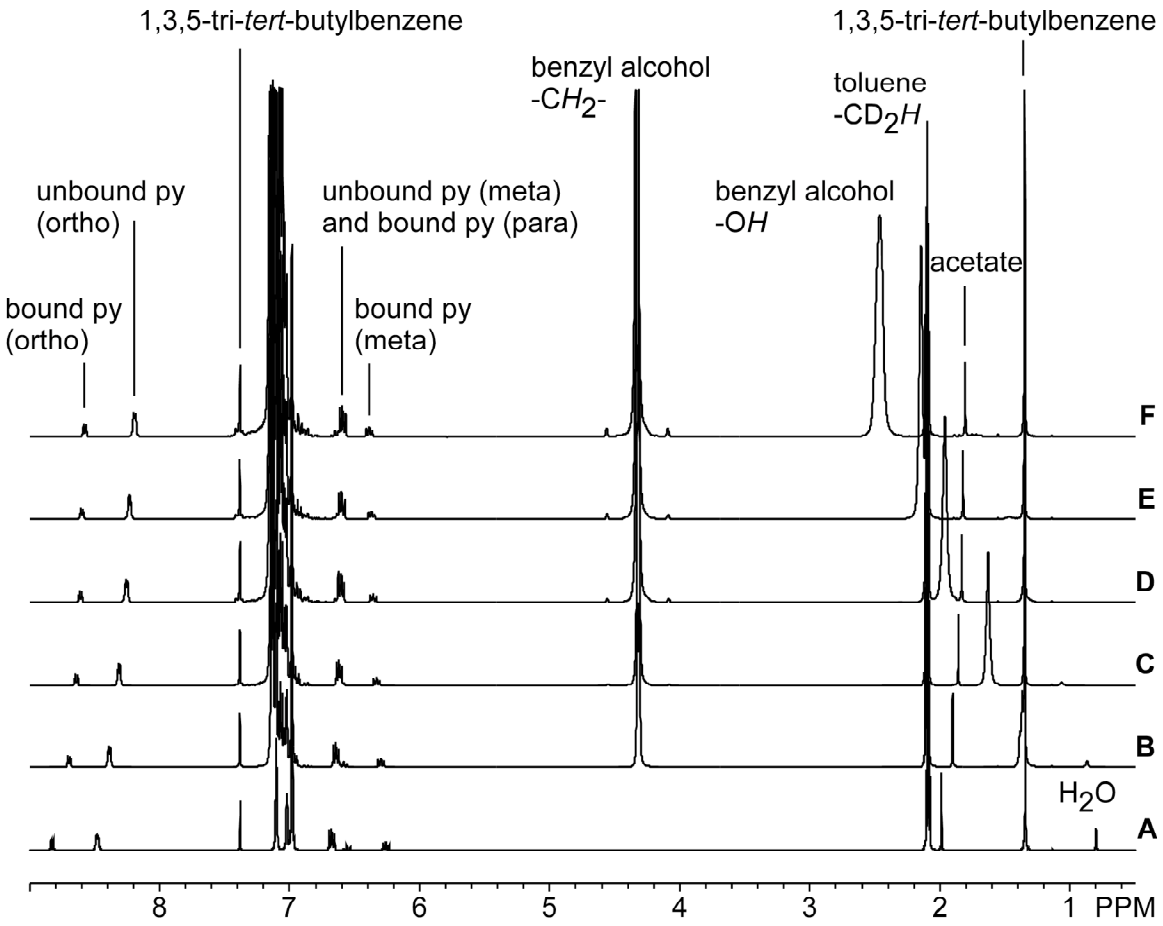

Figure S3. NMR spectra of a titration of benzyl alcohol against $(py)_2Pd(OAc)_2$. Conditions: $[Pd(OAc)_2]$ = 2.2 mM, [pyridine] = 15.1 mM, [alcohol] = 0-460 mM, [1,3,5-tri-*tert*-butylbenzene] = 3.1 mM, toluene-d_8, 22 °C. **A** = 0 M benzyl alcohol. **B** = 0.07 M benzyl alcohol. **C** = 0.18 M benzyl alcohol. **D** = 0.27 M benzyl alcohol. **E** = 0.35 M benzyl alcohol. **F** = 0.46 M benzyl alcohol.

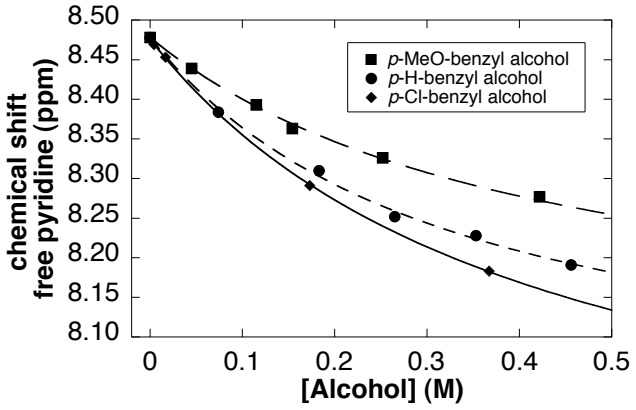

Figure S4. Changes in the unbound pyridine chemical shifts with added 4-methoxybenzyl alcohol, benzyl alcohol, and 4-chlorobenzyl alcohol. Conditions: (A) $[Pd(OAc)_2]$ = 2.5 mM, [pyridine] = 18.8 mM, [4-methoxybenzyl alcohol] = 0-420 mM, [1,3,5-tri-*tert*-butylbenzene] = 2.9 mM, toluene-d_8, 22 °C; squares fit with long dashes. (B) $[Pd(OAc)_2]$ = 2.2 mM, [pyridine] = 15.1 mM, [benzyl alcohol] = 0-460 mM, [1,3,5-tri-*tert*-butylbenzene] = 3.1 mM, toluene-d_8, 22 °C; circles fit with short dashes. (C) $[Pd(OAc)_2]$ = 2.7 mM, [pyridine] = 12.9 mM, [4-chlorobenzyl alcohol] = 0-370 mM, [1,3,5-tri-*tert*-butylbenzene] = 2.2 mM, toluene-d_8, 22 °C; diamonds fit with solid line. Fits were obtained by a nonlinear least-squares fit to eq S13.

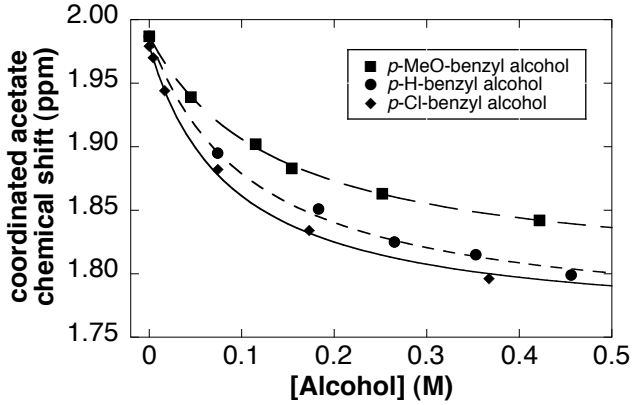

Figure S5. Changes in the acetate chemical shifts with added 4-methoxybenzyl alcohol, benzyl alcohol, and 4-chlorobenzyl alcohol. Conditions: (A) $[Pd(OAc)_2]$ = 2.5 mM, [pyridine] = 18.8 mM, [4-methoxybenzyl alcohol] = 0-420 mM, [1,3,5-tri-*tert*-butylbenzene] = 2.9 mM, toluene-d_8, 22 °C; squares fit with long dashes. (B) $[Pd(OAc)_2]$ = 2.2 mM, [pyridine] = 15.1 mM, [benzyl alcohol] = 0-460 mM, [1,3,5-tri-*tert*-butylbenzene] = 3.1 mM, toluene-d_8, 22 °C; circles fit with short dashes. (C) $[Pd(OAc)_2]$ = 2.7 mM, [pyridine] = 12.9 mM, [4-chlorobenzyl alcohol] = 0-370 mM, [1,3,5-tri-*tert*-butylbenzene] = 2.2 mM, toluene-d_8, 22 °C; diamonds fit with solid line. Fits were obtained by a nonlinear least-squares fit of the bound pyridine (ortho C-H) and the acetate values simultaneously to eq S13.

The derivation of the binding constants for alcohol and 1.

The following equation describes the binding of alcohol to **1**.

$$\underset{\mathbf{1}}{(py)_2Pd(OAc)_2} + RCH_2OH \underset{}{\overset{K_1}{\rightleftharpoons}} \underset{\mathbf{1{\bullet}RCH_2OH}}{(py)_2Pd(OAc)_2(RCH_2OH)} \quad \text{(S1)}$$

The binding constant, K_1, is

$$K_1 = \frac{[\mathbf{1 \bullet RCH_2OH}]}{[\mathbf{1}][RCH_2OH]} \quad \text{(S2)}$$

Since **1** and **1•RCH$_2$OH** exchange rapidly on the NMR timescale, the pyridine and acetate peaks corresponding to **1** and **1•RCH$_2$OH** coalesce. The total concentration of palladium can be determined from the integration of the coalesced peaks and is described as

$$[Pd]_T = [\mathbf{1}] + [\mathbf{1 \bullet RCH_2OH}] \quad \text{(S3)}$$

which can be rearranged in terms of [**1**] so that

$$[\mathbf{1}] = [Pd]_T - [\mathbf{1 \bullet RCH_2OH}] \quad \text{(S4)}$$

The benzylic peak corresponding to RCH$_2$OH and **1•RCH$_2$OH** also coalesce because of rapid exchange. The total concentration of alcohol can be determined from the integration of the coalesced peaks and is described as

$$[ROH]_T = [RCH_2OH] + [\mathbf{1 \bullet RCH_2OH}] \quad \text{(S5)}$$

which can be rearranged in terms of [RCH$_2$OH] so that

$$[RCH_2OH] = [ROH]_T - [\mathbf{1 \bullet RCH_2OH}] \quad \text{(S6)}$$

By substituting eq S4 and eq S6 into eq S2, one obtains

$$K_1 = \frac{[\mathbf{1 \bullet RCH_2OH}]}{([Pd]_T - [\mathbf{1 \bullet RCH_2OH}])([ROH]_T - [\mathbf{1 \bullet RCH_2OH}])} \quad \text{(S7)}$$

which rearranges to

$$K_1[\mathbf{1 \bullet RCH_2OH}]^2 - (K_1[Pd]_T + K_1[ROH]_T + 1)[\mathbf{1 \bullet RCH_2OH}] + K_1[Pd]_T[ROH]_T = 0 \quad \text{(S8)}$$

Application of the quadratic formula allows one to solve eq S8 for [**1•RCH$_2$OH**].

$$[\mathbf{1 \cdot RCH_2OH}] = \frac{K_1[\mathrm{Pd}]_\mathrm{T} + K_1[\mathrm{ROH}]_\mathrm{T} + 1 - \sqrt{(K_1[\mathrm{Pd}]_\mathrm{T} + K_1[\mathrm{ROH}]_\mathrm{T} + 1)^2 - 4K_1^{\,2}[\mathrm{Pd}]_\mathrm{T}[\mathrm{ROH}]_\mathrm{T}}}{2K_1} \qquad \text{(S9)}$$

The molar ratio of the alcohol-catalyst adduct to total palladium is

$$\mathrm{Y}_{\mathbf{1 \cdot RCH_2OH}} = \frac{[\mathbf{1 \cdot RCH_2OH}]}{[\mathbf{1}] + [\mathbf{1 \cdot RCH_2OH}]} = \frac{[\mathbf{1 \cdot RCH_2OH}]}{[\mathrm{Pd}]_\mathrm{T}} \qquad \text{(S10)}$$

By substituting eq S9 into eq S10, one obtains

$$\mathrm{Y}_{\mathbf{1 \cdot RCH_2OH}} = \frac{K_1[\mathrm{Pd}]_\mathrm{T} + K_1[\mathrm{ROH}]_\mathrm{T} + 1 - \sqrt{(K_1[\mathrm{Pd}]_\mathrm{T} + K_1[\mathrm{ROH}]_\mathrm{T} + 1)^2 - 4K_1^{\,2}[\mathrm{Pd}]_\mathrm{T}[\mathrm{ROH}]_\mathrm{T}}}{2K_1[\mathrm{Pd}]_\mathrm{T}} \qquad \text{(S11)}$$

The chemical shift of the coalesced peak corresponding to pyridine or acetate at a given molar ratio of **1•RCH$_2$OH**, $\delta(\mathrm{Pd})^{\mathrm{Y}}$, can be calculated from the molar ratio of **1•RCH$_2$OH** and the chemical shifts of **1** and **1•RCH$_2$OH**. $\delta(\mathrm{Pd})^{\mathbf{1}}$ refers to the chemical shift of **1** with no alcohol present and $\delta(\mathrm{Pd})^{\mathbf{1 \cdot RCH_2OH}}$ refers to the chemical shift of **1•RCH$_2$OH**.

$$\delta(\mathrm{Pd})^{\mathrm{Y}} = \mathrm{Y}_{\mathbf{1 \cdot RCH_2OH}}[\delta(\mathrm{Pd})^{\mathbf{1 \cdot RCH_2OH}} - \delta(\mathrm{Pd})^{\mathbf{1}}] + \delta(\mathrm{Pd})^{\mathbf{1}} \qquad \text{(S12)}$$

By substituting eq S11 into eq S12, one obtains an equation that can be fit to the data in Figures 9B & S4-S5 to determine values for K_1 and $\delta(\mathrm{Pd})^{\mathbf{1 \cdot RCH_2OH}}$.

$$\delta(\mathrm{Pd})^{\mathrm{Y}} = \delta(\mathrm{Pd})^{\mathbf{1}} + \left[\frac{K_1[\mathrm{Pd}]_\mathrm{T} + K_1[\mathrm{ROH}]_\mathrm{T} + 1 - \sqrt{(K_1[\mathrm{Pd}]_\mathrm{T} + K_1[\mathrm{ROH}]_\mathrm{T} + 1)^2 - 4K_1^{\,2}[\mathrm{Pd}]_\mathrm{T}[\mathrm{ROH}]_\mathrm{T}}}{2K_1[\mathrm{Pd}]_\mathrm{T}}\right][\delta(\mathrm{Pd})^{\mathbf{1 \cdot RCH_2OH}} - \delta(\mathrm{Pd})^{\mathbf{1}}] \qquad \text{(S13)}$$

Table S1. Binding Constants of Alcohols to $(py)_2Pd(OAc)_2$.

Alcohol	Temperature (°C)	K_1 (M^{-1})
benzyl alcohol	-75	29.1
	-25	15.2
	0	11.7
	22	9.2
	25	8.7
4-chlorobenzyl alcohol	22	11.5
4-methoxybenzyl alcohol	22	7.4

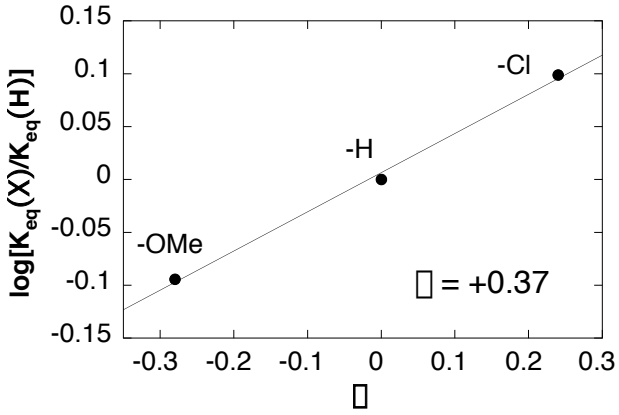

Figure S6. Hammett plot reflecting electronic effect on equilibrium binding of para-substituted benzyl alcohols to $(py)_2Pd(OAc)_2$.

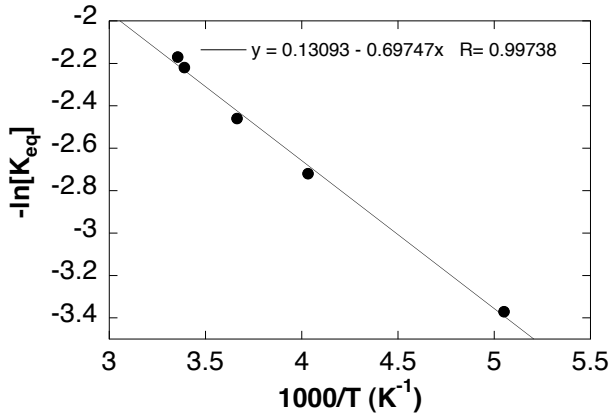

Figure S7. Van't Hoff plot for $PhCH_2OH$ binding to $(py)_2Pd(OAc)_2$ derived from the data in Table S1.

The full NMR spectral timecourse for the oxidation of benzyl alcohol.

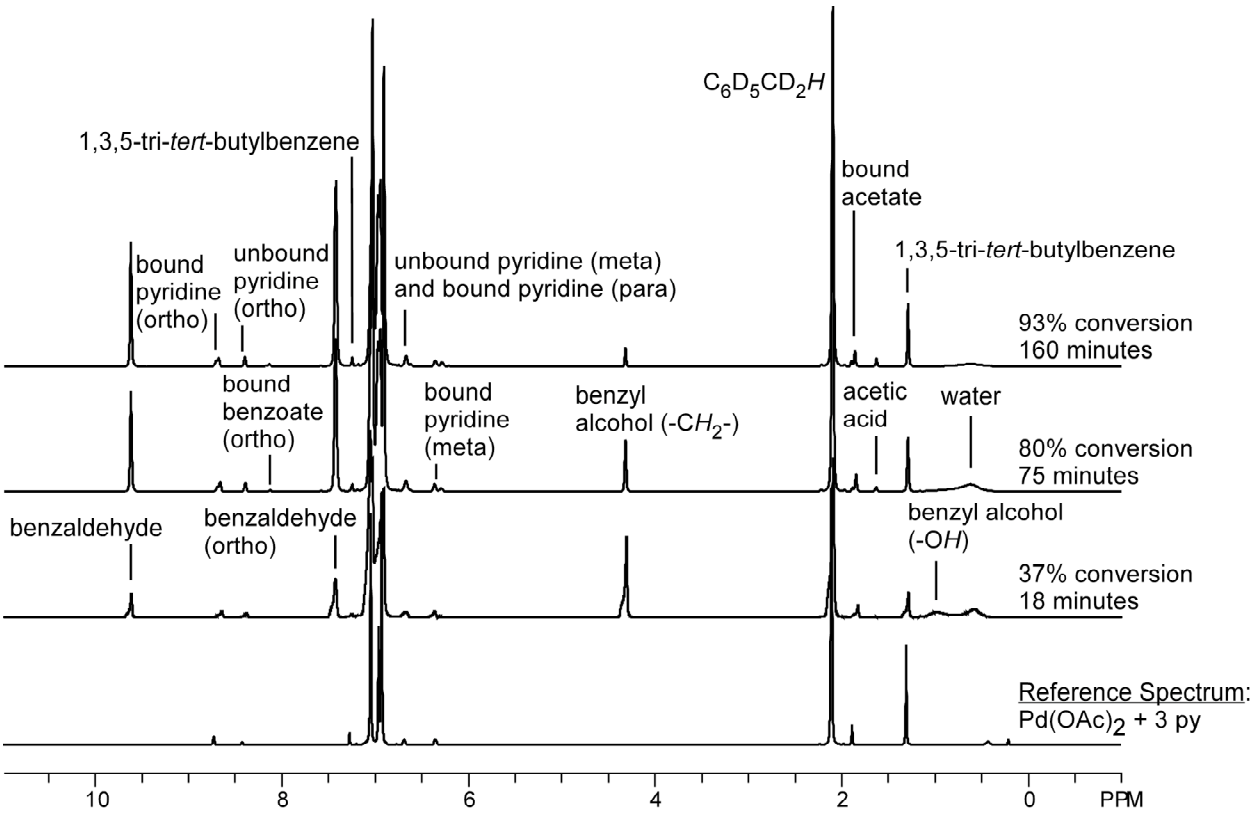

Figure S8. The full NMR spectral timecourse for the oxidation of benzyl alcohol. Conditions: (Reaction) [$Pd(OAc)_2$] = 5.1 mM, [pyridine] = 16.8 mM, [alcohol] = 140 mM, [1,3,5-tri-*tert*-butylbenzene] = 3.0 mM, pO_2 = 10 atm, toluene-d_8, 80 °C. (Reference) [$Pd(OAc)_2$] = 4.8 mM, [pyridine] = 14.0 mM, [1,3,5-tri-*tert*-butylbenzene] = 2.9 mM, pO_2 = 10 atm, toluene-d_8, 80 °C.

Characterization of the equilibrium between $(py)_2Pd(OAc)_2$, $(py)_2Pd(OAc)(O_2CPh)$, and $(py)_2Pd(O_2CPh)_2$.

$$\underset{\mathbf{1}}{(py)_2Pd(OAc)_2} + PhCO_2H \underset{}{\overset{K_{14}}{\rightleftharpoons}} \underset{\mathbf{3}}{(py)_2Pd(OAc)(O_2CPh)} + AcOH \qquad \text{(S14)}$$

$$\underset{\mathbf{3}}{(py)_2Pd(OAc)(O_2CPh)} + PhCO_2H \underset{}{\overset{K_{15}}{\rightleftharpoons}} \underset{\mathbf{4}}{(py)_2Pd(O_2CPh)_2} + AcOH \qquad \text{(S15)}$$

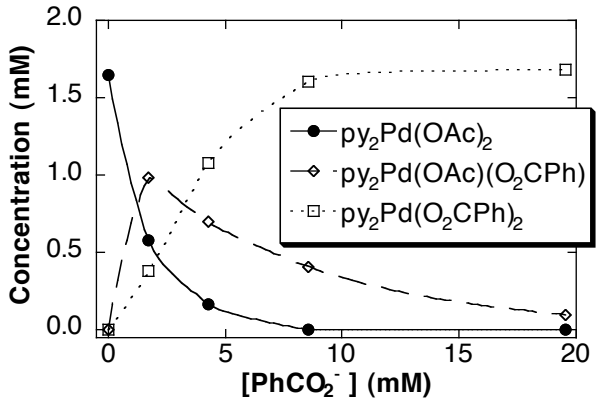

Figure S9. Titration of benzoic acid against $(py)_2Pd(OAc)_2$. Conditions: $[Pd(OAc)_2]$ = 1.8 mM, [pyridine] = 7.6 mM, $[PhCO_2H]$ = 0-19.5 mM, [1,3,5-tri-*tert*-butylbenzene] = 3.0 mM, toluene-d_8, 80 °C.

An example calculation of the equilibrium constants derived from the integrations at 4.3 mM $PhCO_2^-$.

$$K_{14} = \frac{[\text{AcOH}][\mathbf{3}]}{[\text{PhCO}_2\text{H}][\mathbf{1}]} = \frac{3.19 \cdot 0.70}{1.41 \cdot 0.17} = 9.32$$

$$K_{15} = \frac{[\text{AcOH}][\mathbf{4}]}{[\text{PhCO}_2\text{H}][\mathbf{3}]} = \frac{3.19 \cdot 1.08}{1.41 \cdot 0.70} = 3.49$$

The full NMR spectral timecourse for the oxidation of *sec*-phenethyl alcohol.

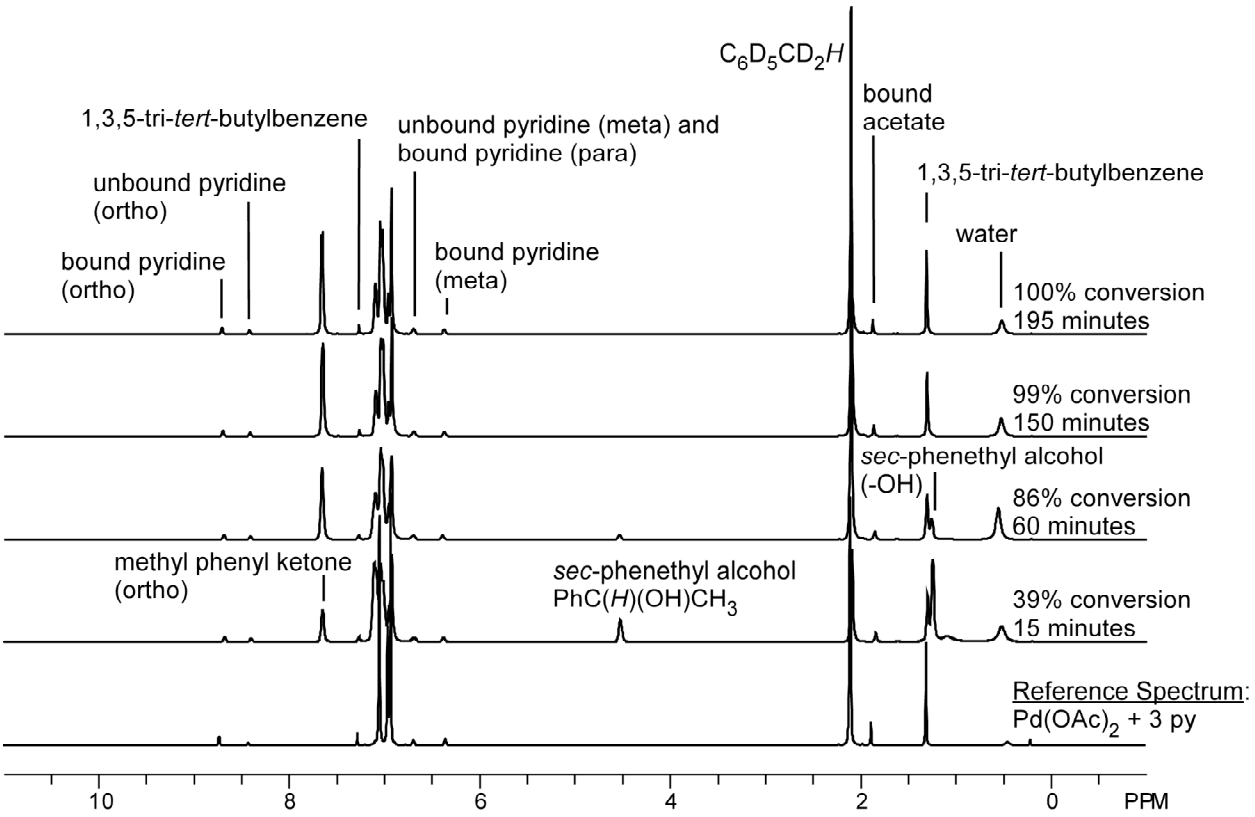

Figure S10. The full NMR spectral timecourse for the oxidation of *sec*-phenethyl alcohol. Conditions: (Reaction) $[Pd(OAc)_2]$ = 4.5 mM, [pyridine] = 15.3 mM, [alcohol] = 150 mM, [1,3,5-tri-*tert*-butylbenzene] = 2.6 mM, pO_2 = 10 atm, toluene-d_8, 80 °C. (Reference) $[Pd(OAc)_2]$ = 4.8 mM, [pyridine] = 14.0 mM, [1,3,5-tri-*tert*-butylbenzene] = 2.9 mM, pO_2 = 10 atm, toluene-d_8, 80 °C.

Alcohol concentration dependence for a series of *para*-substituted benzyl alcohols.

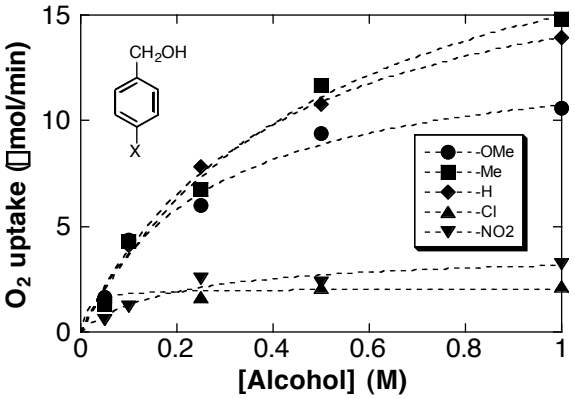

Figure S11. Initial rate dependence on alcohol concentration for a series of *para*-substituted benzyl alcohols. Conditions: $[Pd(OAc)_2]$ = 2.5 mM, [pyridine] = 10 mM, [alcohol] = 0.05-1.0 M, pO_2 = 700 torr, 80 °C.

Hammett plots for a series of *para*-substituted benzyl alcohols.

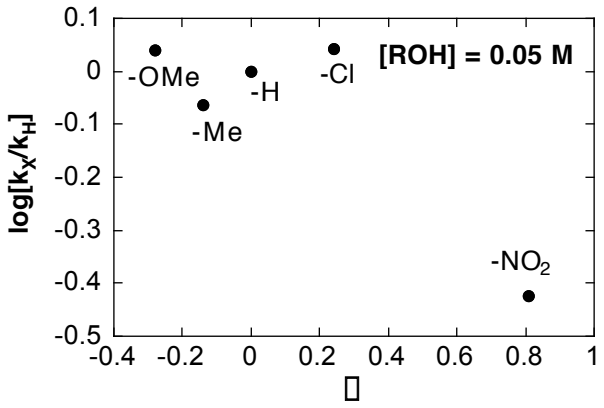

Figure S12. Hammett plot derived from the relative initial rates of catalytic alcohol oxidation conducted with a series of *para*-substituted benzyl alcohols at 0.05 M alcohol. Conditions: $[Pd(OAc)_2]$ = 2.5 mM, [pyridine] = 10 mM, [alcohol] = 0.05 M, pO_2 = 700 torr, 80 °C.

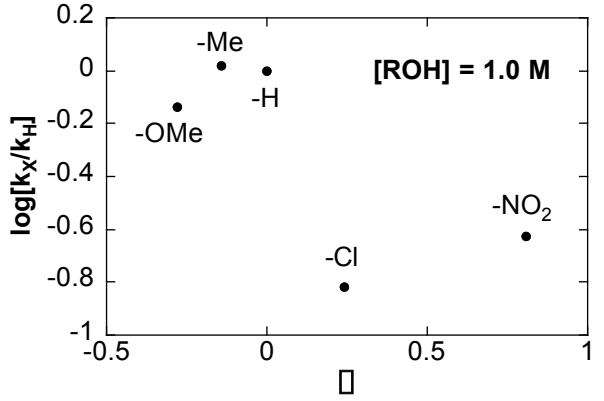

Figure S13. Hammett plot derived from the relative initial rates of catalytic alcohol oxidation conducted with a series of *para*-substituted benzyl alcohols at 1.0 M alcohol. Conditions: $[Pd(OAc)_2]$ = 2.5 mM, [pyridine] = 10 mM, [alcohol] = 1.0 M, pO_2 = 700 torr, 80 °C.

Rate law derivations.

The rate law corresponding to the mechanism described in the text (eq 16) is modified from what has been derived previously.[1] The following derivation adds the additional step for the formation of an alcohol-catalyst adduct.

The following mechanism (Scheme 3) accounts for the experimental observations.

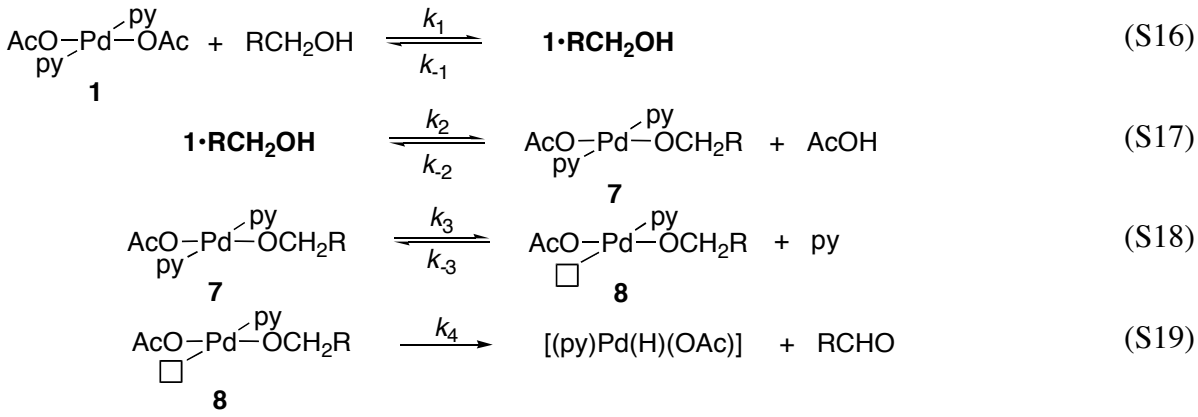

The rate of product formation is described by the following rate law.

$$\text{Rate} = \frac{d[\text{RCHO}]}{dt} = k_4[\mathbf{8}] \tag{S20}$$

Since **1** and **1•RCH$_2$OH** exchange rapidly on the NMR timescale, their relationship can be described as a rapid pre-equilibrium.

$$K_1 = \frac{[\mathbf{1 \bullet RCH_2OH}]}{[\mathbf{1}][\text{PhCH}_2\text{OH}]} \tag{S21}$$

According to the steady-state approximation, [**7**] and [**8**] can be described as

$$[\mathbf{7}]_{ss} = \frac{k_2[\mathbf{1 \bullet RCH_2OH}] + k_{\square 3}[\mathbf{8}][\text{py}]}{k_{\square 2}[\text{AcOH}] + k_3} \tag{S22}$$

$$[\mathbf{8}]_{ss} = \frac{k_3[\mathbf{7}]}{k_{\square 3}[\text{py}] + k_4} \tag{S23}$$

If one assumes that [**7**] and [**8**] are vanishingly small and do not contribute to the steady state palladium concentration, $[Pd]_T$, then

$$[Pd]_T = [\mathbf{1}] + [\mathbf{1} \bullet \mathbf{RCH_2OH}] \tag{S24}$$

which can be rearranged in terms of [**1**] so that

$$[\mathbf{1}] = [Pd]_T - [\mathbf{1} \bullet \mathbf{RCH_2OH}] \tag{S25}$$

By substituting eq S25 into eq S21, one obtains

$$K_1 = \frac{[\mathbf{1} \bullet \mathbf{RCH_2OH}]}{([Pd]_T - [\mathbf{1} \bullet \mathbf{RCH_2OH}])[PhCH_2OH]} \tag{S26}$$

which rearranges to

$$[\mathbf{1} \bullet \mathbf{RCH_2OH}] = \frac{K_1[Pd]_T[PhCH_2OH]}{1 + K_1[PhCH_2OH]} \tag{S27}$$

By substituting eq S27 into eq S22, one obtains

$$[\mathbf{7}] = \frac{k_2\left(\frac{K_1[Pd]_T[PhCH_2OH]}{1 + K_1[PhCH_2OH]}\right) + k_{-3}[\mathbf{8}][py]}{k_{-2}[AcOH] + k_3} \tag{S28}$$

By substituting eq S28 into eq S23, one obtains

$$[\mathbf{8}] = \frac{k_3}{k_{-3}[py] + k_4} \cdot \left(\frac{k_2\left(\frac{K_1[Pd]_T[PhCH_2OH]}{1 + K_1[PhCH_2OH]}\right) + k_{-3}[\mathbf{8}][py]}{k_{-2}[AcOH] + k_3}\right) \tag{S29}$$

and by solving eq S29 for [**8**], one obtains

$$[\mathbf{8}] = \frac{k_2k_3\left(\frac{K_1[Pd]_T[PhCH_2OH]}{1 + K_1[PhCH_2OH]}\right)}{(k_{-2}[AcOH] + k_3)(k_{-3}[py] + k_4) - k_3k_{-3}[py]} \tag{S30}$$

which simplifies to

$$[\mathbf{8}] = \frac{K_1 k_2 k_3 [\mathrm{Pd}]_T [\mathrm{PhCH_2OH}]}{(1 + K_1[\mathrm{PhCH_2OH}])(k_{-2}[\mathrm{AcOH}](k_{-3}[\mathrm{py}] + k_4) + k_3 k_4)} \tag{S31}$$

Substitution of eq S31 into eq S20 yields the rate law (eq 16).

$$\mathrm{Rate} = \frac{K_1 k_2 k_3 k_4 [\mathrm{Pd}]_T [\mathrm{PhCH_2OH}]}{(1 + K_1[\mathrm{PhCH_2OH}])(k_{-2}[\mathrm{AcOH}](k_{-3}[\mathrm{py}] + k_4) + k_3 k_4)} \tag{S32}$$

The rate law corresponding to the mechanism described in the text (eq 16) predicts a first-order dependence on [palladium]. The following derivation reveals the origin of the half-order [palladium] dependence when the reaction is conducted in the presence of a large excess of pyridine.

If no acetic acid is added to the reaction, then the steady state concentration of acetic acid can be equated to the concentration of **7** according to the equilibrium described in eq S17.

$$[\mathrm{AcOH}] = [\mathbf{7}] \tag{S33}$$

Eq S28 can be rewritten to substitute for the steady state concentration of acetic acid.

$$[\mathbf{7}] = \frac{k_2 \left(\frac{K_1 [\mathrm{Pd}]_T [\mathrm{PhCH_2OH}]}{1 + K_1[\mathrm{PhCH_2OH}]} \right) + k_{-3}[\mathbf{8}][\mathrm{py}]}{k_{-2}[\mathbf{7}] + k_3} \tag{S34}$$

Eq S34 rearranges to

$$k_{-2}[\mathbf{7}]^2 + k_3[\mathbf{7}] - \left(k_2 \left(\frac{K_1 [\mathrm{Pd}]_T [\mathrm{PhCH_2OH}]}{1 + K_1[\mathrm{PhCH_2OH}]} \right) + k_{-3}[\mathbf{8}][\mathrm{py}] \right) = 0 \tag{S35}$$

Application of the quadratic formula allows one to solve eq S35 for [**7**].

$$[\mathbf{7}] = \frac{-k_3 + \sqrt{k_3^{\,2} + 4k_{-2}\left(k_2 \left(\frac{K_1 [\mathrm{Pd}]_T [\mathrm{PhCH_2OH}]}{1 + K_1[\mathrm{PhCH_2OH}]} \right) + k_{-3}[\mathbf{8}][\mathrm{py}] \right)}}{2k_{-2}} \tag{S36}$$

By substituting eq S36 into eq S23, one obtains

$$[\mathbf{8}] = \frac{k_3}{k_{\square 3}[\mathrm{py}] + k_4} \cdot \left(\frac{-k_3 + \sqrt{k_3^{\,2} + 4k_{\square 2}\left(k_2 \frac{K_1[\mathrm{Pd}]_\mathrm{T}[\mathrm{PhCH_2OH}]}{1 + K_1[\mathrm{PhCH_2OH}]} + k_{\square 3}[\mathbf{8}][\mathrm{py}]\right)}}{2k_{\square 2}} \right) \tag{S37}$$

which rearranges to

$$\left(\frac{k_{\square 2}(k_{\square 3}[\mathrm{py}] + k_4)^2}{k_3^{\,2}} \right)[\mathbf{8}]^2 + k_4[\mathbf{8}] - k_2 \left(\frac{K_1[\mathrm{Pd}]_\mathrm{T}[\mathrm{PhCH_2OH}]}{1 + K_1[\mathrm{PhCH_2OH}]} \right) = 0 \tag{S38}$$

Application of the quadratic formula allows one to solve eq S38 for [**8**].

$$[\mathbf{8}] = \frac{k_3 \left(-k_3k_4 + \sqrt{k_3^{\,2}k_4^{\,2} + 4k_2k_{\square 2}(k_{\square 3}[\mathrm{py}] + k_4)^2 \left(\frac{K_1[\mathrm{Pd}]_\mathrm{T}[\mathrm{PhCH_2OH}]}{1 + K_1[\mathrm{PhCH_2OH}]} \right)} \right)}{2k_{\square 2}(k_{\square 3}[\mathrm{py}] + k_4)^2} \tag{S39}$$

The rate law can now be solved with the $[\mathrm{Pd}]_\mathrm{T}$ term under the square root.

$$\mathrm{Rate} = \frac{k_3k_4 \left(-k_3k_4 + \sqrt{k_3^{\,2}k_4^{\,2} + 4k_2k_{\square 2}(k_{\square 3}[\mathrm{py}] + k_4)^2 \left(\frac{K_1[\mathrm{Pd}]_\mathrm{T}[\mathrm{PhCH_2OH}]}{1 + K_1[\mathrm{PhCH_2OH}]} \right)} \right)}{2k_{\square 2}(k_{\square 3}[\mathrm{py}] + k_4)^2} \tag{S40}$$

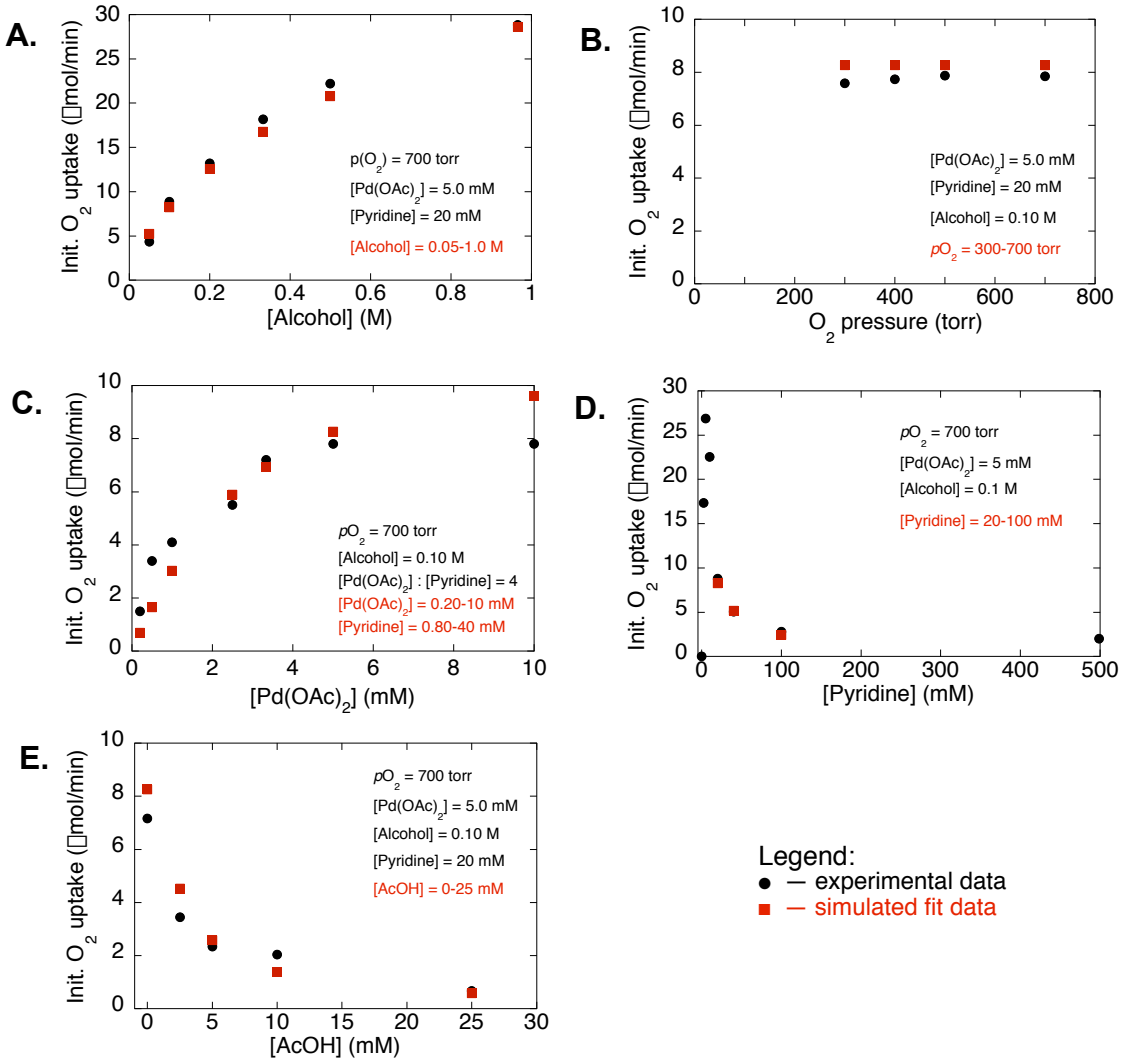

Figure S14. Results of a simultaneous fit of the kinetics data in Figures 2-5 and 7 to the rate laws in eqs 16 and S40. Eq S40 is used to fit data from reactions in which no exogenous acetic acid is included (Figures S14A-D and the [AcOH] = 0 point in Figure S14E). Kinetics data acquired at low and high [pyridine] (plot D) were not included in the fit: at [py] ≤ 10 mM, the lack of free pyridine (i.e., [py] = 0) causes the fit to fail, and at high [py], a parallel mechanism involving β-hydride elimination from 4-coordinate palladium appears to be operating, but is not included in the rate expression. The constants derived from the fit ($K_1 = 0.23$, $k_2 = 1.6\text{x}10^5$, $k_{-2} = 1.0\text{x}10^7$, $k_3 = 1.4\text{x}10^4$, $k_{-3} = 6.8\text{x}10^3$, $k_4 = 104$) are not significant in an absolute sense because of the high degree of correlation.

Single crystal X-ray crystallography for $[NBu_4]^+[AcO\cdots HOAc]^-$ (2).

Data Collection

A colorless crystal with approximate dimensions 0.50 x 0.41 x 0.33 mm^3 was selected under oil under ambient conditions and attached to the tip of a glass capillary. The crystal was mounted in a stream of cold nitrogen at 100(2) K and centered in the X-ray beam by using a video camera.

The crystal evaluation and data collection were performed on a Bruker CCD-1000 diffractometer with Mo K_α (λ = 0.71073 Å) radiation and the diffractometer to crystal distance of 4.9 cm.

The initial cell constants were obtained from three series of ω scans at different starting angles. Each series consisted of 20 frames collected at intervals of 0.3º in a 6º range about ω with the exposure time of 20 seconds per frame. A total of 65 reflections was obtained. The reflections were successfully indexed by an automated indexing routine built in the SMART program. The final cell constants were calculated from a set of 5761 strong reflections from the actual data collection.

The data were collected by using the hemisphere data collection routine. The reciprocal space was surveyed to the extent of a full sphere to a resolution of 0.80 Å. A total of 9093 data were harvested by collecting three sets of frames with 0.3º scans in ω with an exposure time 30 sec per frame. These highly redundant datasets were corrected for Lorentz and polarization effects. The absorption correction was based on fitting a function to the empirical transmission surface as sampled by multiple equivalent measurements.[2]

Structure Solution and Refinement

The systematic absences in the diffraction data were consistent for the space groups $P\bar{1}$ and $P1$. The *E*-statistics strongly suggested the centrosymmetric space group $P\bar{1}$ that yielded chemically reasonable and computationally stable results of refinement.[2] A successful solution by the direct methods provided most non-hydrogen atoms from the *E*-map. The remaining non-hydrogen atoms were located in an alternating series of least-squares cycles and difference Fourier maps. All non-hydrogen atoms were refined with anisotropic displacement coefficients. All hydrogen atoms were independently refined with isotropic displacement coefficients.

The compositions of the unit cell is $[N(n\text{-}Bu)_4]^+[AcOH\ldots OAc]^-$. Each anion $[AcOH\ldots OAc]^-$ occupies a crystallographic inversion center.

The final least-squares refinement of 402 parameters against 4464 data resulted in residuals *R* (based on F^2 for $I \geq 2\sigma$) and *wR* (based on F^2 for all data) of 0.0498 and 0.1175, respectively. The final difference Fourier map was featureless.

The ORTEP diagram is drawn with 50% probability ellipsoids.

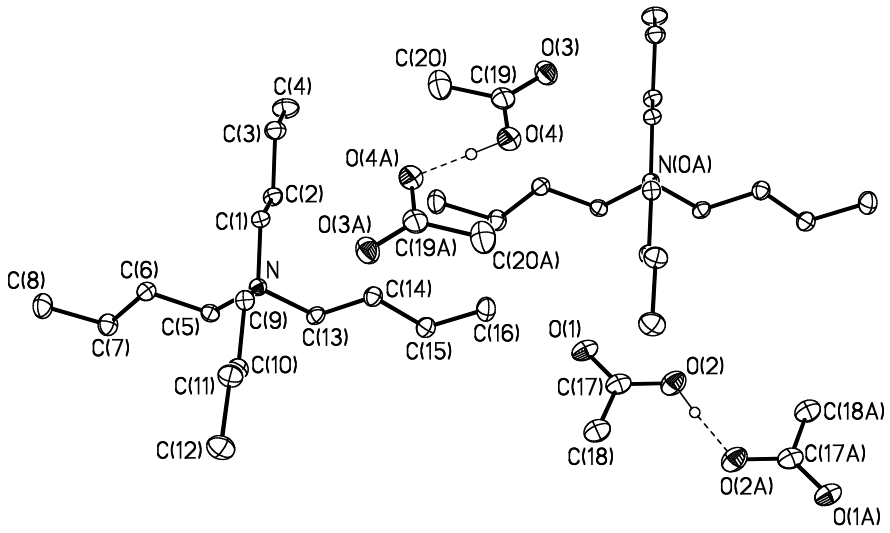

Figure S15. ORTEP diagram of **2**.

Table S2. Crystal data and structure refinement for **2**.

Empirical formula	$C_{20}H_{43}NO_4$	
Formula weight	361.55	
Temperature	100(2) K	
Wavelength	0.71073 Å	
Crystal system	Triclinic	
Space group	*P*1	
Unit cell dimensions	a = 9.4445(16) Å	□= 86.959(3)°.
	b = 9.4856(16) Å	□= 85.645(3)°.
	c = 12.352(2) Å	□= 89.977(3)°.
Volume	1101.8(3) Å^3	
Z	2	
Density (calculated)	1.090 Mg/m^3	
Absorption coefficient	0.074 mm^{-1}	
F(000)	404	
Crystal size	0.50 x 0.41 x 0.33 mm^3	
Theta range for data collection	1.66 to 26.40°.	
Index ranges	-11<=h<=11, -11<=k<=11, -15<=l<=15	
Reflections collected	9093	
Independent reflections	4464 [R(int) = 0.0239]	
Completeness to theta = 26.40°	98.8 %	
Absorption correction	Multiscan with SADABS	
Max. and min. transmission	0.9761 and 0.9640	
Refinement method	Full-matrix least-squares on F^2	
Data / restraints / parameters	4464 / 0 / 402	
Goodness-of-fit on F^2	1.164	
Final R indices [I>2sigma(I)]	R1 = 0.0498, wR2 = 0.1149	
R indices (all data)	R1 = 0.0564, wR2 = 0.1175	
Largest diff. peak and hole	0.244 and -0.190 e.Å^{-3}	

Table S3. Bond lengths [Å] and angles [°] for (**2**).

O(1)-C(17)	1.228(2)	C(8)-H(8C)	1.00(2)
O(2)-C(17)	1.297(2)	C(9)-C(10)	1.516(2)
O(2)-H(2)	0.89(4)	C(9)-H(9A)	0.953(18)
O(3)-C(19)	1.230(2)	C(9)-H(9B)	0.965(17)
O(4)-C(19)	1.292(2)	C(10)-C(11)	1.527(2)
O(4)-H(4)	0.93(7)	C(10)-H(10A)	0.967(19)
N-C(13)	1.5204(19)	C(10)-H(10B)	0.961(18)
N-C(5)	1.5220(19)	C(11)-C(12)	1.522(2)
N-C(1)	1.5232(19)	C(11)-H(11A)	0.94(2)
N-C(9)	1.5237(19)	C(11)-H(11B)	0.99(2)
C(1)-C(2)	1.519(2)	C(12)-H(12A)	0.96(2)
C(1)-H(1A)	0.940(18)	C(12)-H(12B)	0.97(2)
C(1)-H(1B)	0.959(17)	C(12)-H(12C)	0.99(2)
C(2)-C(3)	1.529(2)	C(13)-C(14)	1.511(2)
C(2)-H(2A)	0.966(17)	C(13)-H(13A)	0.974(17)
C(2)-H(2B)	0.974(18)	C(13)-H(13B)	0.959(17)
C(3)-C(4)	1.521(2)	C(14)-C(15)	1.527(2)
C(3)-H(3A)	0.974(19)	C(14)-H(14A)	0.96(2)
C(3)-H(3B)	0.965(19)	C(14)-H(14B)	0.967(19)
C(4)-H(4A)	0.99(2)	C(15)-C(16)	1.521(2)
C(4)-H(4B)	0.94(2)	C(15)-H(15A)	0.970(19)
C(4)-H(4C)	1.01(2)	C(15)-H(15B)	0.95(2)
C(5)-C(6)	1.515(2)	C(16)-H(16A)	0.98(2)
C(5)-H(5A)	0.946(18)	C(16)-H(16B)	0.95(2)
C(5)-H(5B)	0.976(17)	C(16)-H(16C)	0.98(2)
C(6)-C(7)	1.533(2)	C(17)-C(18)	1.512(3)
C(6)-H(6A)	0.948(18)	C(18)-H(18A)	0.97(3)
C(6)-H(6B)	0.987(18)	C(18)-H(18B)	0.94(3)
C(7)-C(8)	1.522(2)	C(18)-H(18C)	0.94(3)
C(7)-H(7A)	0.98(2)	C(19)-C(20)	1.514(3)
C(7)-H(7B)	0.974(18)	C(20)-H(20A)	0.94(4)
C(8)-H(8A)	0.96(2)	C(20)-H(20B)	0.89(4)
C(8)-H(8B)	0.96(2)	C(20)-H(20C)	0.89(4)

C(17)-O(2)-H(2)	116(3)	C(2)-C(3)-H(3A)	108.5(11)
C(19)-O(4)-H(4)	114(5)	C(4)-C(3)-H(3B)	109.3(11)
C(13)-N-C(5)	104.91(11)	C(2)-C(3)-H(3B)	108.6(11)
C(13)-N-C(1)	111.63(11)	H(3A)-C(3)-H(3B)	108.4(15)
C(5)-N-C(1)	111.86(11)	C(3)-C(4)-H(4A)	109.1(12)
C(13)-N-C(9)	111.72(11)	C(3)-C(4)-H(4B)	110.2(14)
C(5)-N-C(9)	112.13(12)	H(4A)-C(4)-H(4B)	108.2(18)
C(1)-N-C(9)	104.77(11)	C(3)-C(4)-H(4C)	111.0(12)
C(2)-C(1)-N	115.86(12)	H(4A)-C(4)-H(4C)	109.5(17)
C(2)-C(1)-H(1A)	110.9(10)	H(4B)-C(4)-H(4C)	108.8(18)
N-C(1)-H(1A)	105.2(10)	C(6)-C(5)-N	116.51(12)
C(2)-C(1)-H(1B)	109.6(10)	C(6)-C(5)-H(5A)	109.8(10)
N-C(1)-H(1B)	105.3(10)	N-C(5)-H(5A)	105.3(10)
H(1A)-C(1)-H(1B)	109.7(14)	C(6)-C(5)-H(5B)	110.0(10)
C(1)-C(2)-C(3)	109.37(13)	N-C(5)-H(5B)	104.9(10)
C(1)-C(2)-H(2A)	111.1(10)	H(5A)-C(5)-H(5B)	110.0(14)
C(3)-C(2)-H(2A)	107.2(10)	C(5)-C(6)-C(7)	107.95(13)
C(1)-C(2)-H(2B)	111.7(10)	C(5)-C(6)-H(6A)	112.5(11)
C(3)-C(2)-H(2B)	108.7(10)	C(7)-C(6)-H(6A)	108.4(11)
H(2A)-C(2)-H(2B)	108.7(14)	C(5)-C(6)-H(6B)	111.5(10)
C(4)-C(3)-C(2)	112.03(14)	C(7)-C(6)-H(6B)	108.9(10)
C(4)-C(3)-H(3A)	110.0(11)	H(6A)-C(6)-H(6B)	107.5(15)

C(8)-C(7)-C(6)	113.03(14)
C(8)-C(7)-H(7A)	108.2(11)
C(6)-C(7)-H(7A)	108.7(11)
C(8)-C(7)-H(7B)	109.2(10)
C(6)-C(7)-H(7B)	109.0(10)
H(7A)-C(7)-H(7B)	108.5(15)
C(7)-C(8)-H(8A)	110.6(12)
C(7)-C(8)-H(8B)	110.4(12)
H(8A)-C(8)-H(8B)	107.9(17)
C(7)-C(8)-H(8C)	109.9(12)
H(8A)-C(8)-H(8C)	108.8(17)
H(8B)-C(8)-H(8C)	109.2(17)
C(10)-C(9)-N	116.40(12)
C(10)-C(9)-H(9A)	110.9(10)
N-C(9)-H(9A)	104.9(10)
C(10)-C(9)-H(9B)	111.5(10)
N-C(9)-H(9B)	104.8(10)
H(9A)-C(9)-H(9B)	107.8(14)
C(9)-C(10)-C(11)	108.66(13)
C(9)-C(10)-H(10A)	110.9(11)
C(11)-C(10)-H(10A)	109.4(11)
C(9)-C(10)-H(10B)	110.9(10)
C(11)-C(10)-H(10B)	109.8(10)
H(10A)-C(10)-H(10B)	107.3(15)
C(12)-C(11)-C(10)	113.07(14)
C(12)-C(11)-H(11A)	109.6(12)
C(10)-C(11)-H(11A)	109.1(12)
C(12)-C(11)-H(11B)	109.1(11)
C(10)-C(11)-H(11B)	109.1(11)
H(11A)-C(11)-H(11B)	106.7(16)
C(11)-C(12)-H(12A)	112.0(12)
C(11)-C(12)-H(12B)	111.1(12)
H(12A)-C(12)-H(12B)	105.8(17)
C(11)-C(12)-H(12C)	110.5(12)
H(12A)-C(12)-H(12C)	105.8(17)
H(12B)-C(12)-H(12C)	111.3(17)
C(14)-C(13)-N	115.82(12)
C(14)-C(13)-H(13A)	111.1(10)
N-C(13)-H(13A)	104.6(10)
C(14)-C(13)-H(13B)	110.7(10)
N-C(13)-H(13B)	106.1(10)
H(13A)-C(13)-H(13B)	108.1(14)
C(13)-C(14)-C(15)	110.08(13)
C(13)-C(14)-H(14A)	109.5(11)
C(15)-C(14)-H(14A)	110.4(11)
C(13)-C(14)-H(14B)	111.7(11)
C(15)-C(14)-H(14B)	107.3(11)
H(14A)-C(14)-H(14B)	107.8(16)
C(16)-C(15)-C(14)	112.06(14)
C(16)-C(15)-H(15A)	108.9(11)
C(14)-C(15)-H(15A)	110.5(11)
C(16)-C(15)-H(15B)	108.6(12)
C(14)-C(15)-H(15B)	110.6(12)
H(15A)-C(15)-H(15B)	106.0(16)
C(15)-C(16)-H(16A)	111.0(12)
C(15)-C(16)-H(16B)	111.5(13)
H(16A)-C(16)-H(16B)	110.6(17)
C(15)-C(16)-H(16C)	110.8(12)
H(16A)-C(16)-H(16C)	104.9(17)
H(16B)-C(16)-H(16C)	107.9(17)
O(1)-C(17)-O(2)	122.52(16)
O(1)-C(17)-C(18)	120.80(17)
O(2)-C(17)-C(18)	116.68(16)
C(17)-C(18)-H(18A)	109.2(17)
C(17)-C(18)-H(18B)	112.1(17)
H(18A)-C(18)-H(18B)	104(2)
C(17)-C(18)-H(18C)	111.9(16)
H(18A)-C(18)-H(18C)	109(2)
H(18B)-C(18)-H(18C)	111(2)
O(3)-C(19)-O(4)	122.74(17)
O(3)-C(19)-C(20)	120.27(18)
O(4)-C(19)-C(20)	116.98(17)
C(19)-C(20)-H(20A)	112(2)
C(19)-C(20)-H(20B)	112(2)
H(20A)-C(20)-H(20B)	106(3)
C(19)-C(20)-H(20C)	109(2)
H(20A)-C(20)-H(20C)	114(3)
H(20B)-C(20)-H(20C)	103(3)

Table S4. Hydrogen bonds for (**2**) [Å and °].

D-H...A	d(D-H)	d(H...A)	d(D...A)	<(DHA)
O(2)-H(2)...O(2)#1	0.89(4)	1.57(4)	2.455(3)	171(5)
O(4)-H(4)...O(4)#2	0.93(7)	1.52(7)	2.455(3)	173(8)

Symmetry transformations used to generate equivalent atoms:
#1 -x+2,-y+2,-z #2 -x+1,-y+1,-z+1

Single crystal X-ray crystallography for $(py)_2Pd(O_2CPh)_2$ (4).

Data Collection

A yellow crystal with approximate dimensions 0.44 x 0.26 x 0.21 mm^3 was selected under oil under ambient conditions and attached to the tip of a nylon loop. The crystal was mounted in a stream of cold nitrogen at 100(2) K and centered in the X-ray beam by using a video camera.

The crystal evaluation and data collection were performed on a Bruker CCD-1000 diffractometer with Mo K_α (λ = 0.71073 Å) radiation and the diffractometer to crystal distance of 4.9 cm.

The initial cell constants were obtained from three series of ω scans at different starting angles. Each series consisted of 20 frames collected at intervals of 0.3º in a 6º range about ω with the exposure time of 15 seconds per frame. A total of 81 reflections was obtained. The reflections were successfully indexed by an automated indexing routine built in the SMART program. The final cell constants were calculated from a set of 5586 strong reflections from the actual data collection.

The data were collected by using the hemisphere data collection routine. The reciprocal space was surveyed to the extent of a full sphere to a resolution of 0.80 Å. A total of 8240 data were harvested by collecting three sets of frames with 0.25º scans in ω with an exposure time 60 sec per frame. These highly redundant datasets were corrected for Lorentz and polarization effects. The absorption correction was based on fitting a function to the empirical transmission surface as sampled by multiple equivalent measurements.[2]

Structure Solution and Refinement

The systematic absences in the diffraction data were consistent for the space groups $P2_1/m$ and $P2_1$. The *E*-statistics strongly suggested the non-centrosymmetric space group $P2_1$ that yielded chemically reasonable and computationally stable results of refinement.[2] A successful solution by the direct methods provided most non-hydrogen atoms from the *E*-map. The remaining non-hydrogen atoms were located in an alternating series of least-squares cycles and difference Fourier maps. All non-hydrogen atoms were refined with anisotropic displacement coefficients. All hydrogen atoms were included in the structure factor calculation at idealized positions and were allowed to ride on the neighboring atoms with relative isotropic displacement coefficients. The complex is a merohedral twin with a 0.55/0.45 component ratio. There is no inversion center in the molecule.

The final least-squares refinement of 281 parameters against 4158 data resulted in residuals *R* (based on F^2 for $I \geq 2\sigma$) and *wR* (based on F^2 for all data) of 0.0423 and 0.1042, respectively. The final difference Fourier map was featureless.

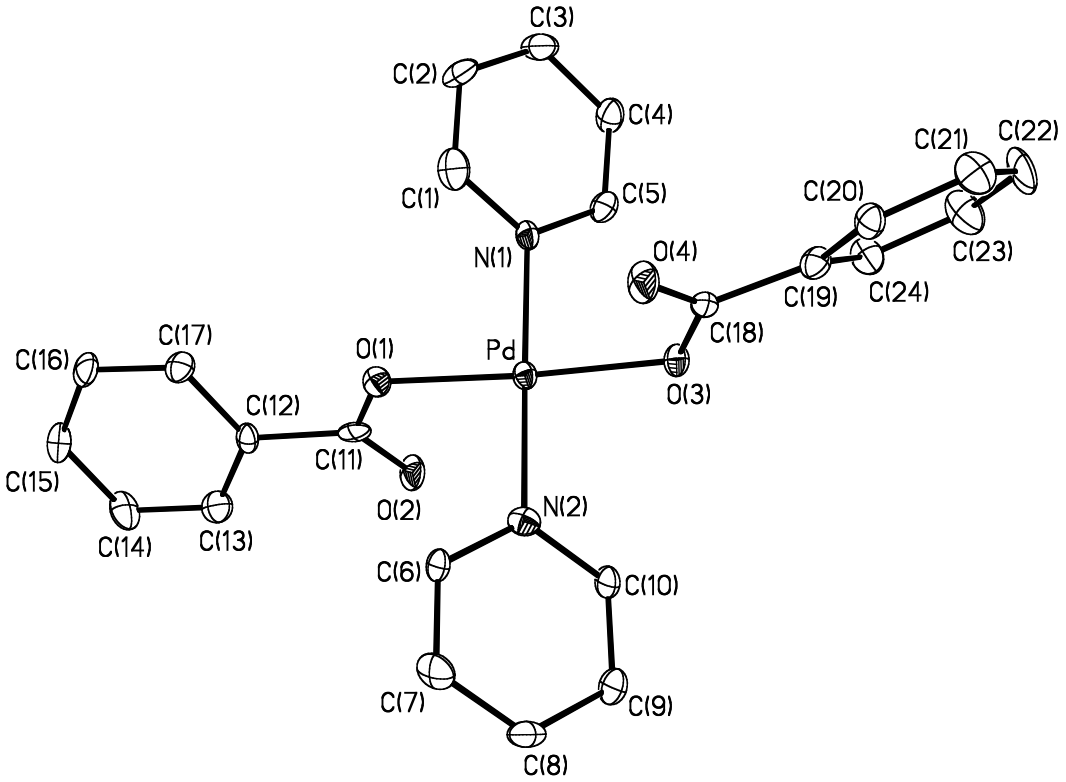

Figure S16. ORTEP diagram of **4** drawn with 50% probability ellipsoids.

Table S5. Crystal data and structure refinement for (**4**).

Empirical formula	$C_{24}H_{20}N_2O_4Pd$	
Formula weight	506.82	
Temperature	100(2) K	
Wavelength	0.71073 Å	
Crystal system	Monoclinic	
Space group	$P2_1$	
Unit cell dimensions	a = 10.928(2) Å	□= 90°.
	b = 9.2369(18) Å	□= 109.070(3)°.
	c = 11.087(2) Å	□= 90°.
Volume	1057.7(4) $Å^3$	
Z	2	
Density (calculated)	1.591 Mg/m^3	
Absorption coefficient	0.911 mm^{-1}	
F(000)	512	
Crystal size	0.44 x 0.26 x 0.21 mm^3	
Theta range for data collection	1.94 to 26.43°.	
Index ranges	-13<=h<=13, -11<=k<=11, -13<=l<=13	
Reflections collected	8240	
Independent reflections	4158 [R(int) = 0.0298]	
Completeness to theta = 26.43°	98.9 %	
Absorption correction	Multiscan with SADABS	

Max. and min. transmission	0.8317 and 0.6900
Refinement method	Full-matrix least-squares on F^2
Data / restraints / parameters	4158 / 13 / 281
Goodness-of-fit on F^2	1.052
Final R indices [I>2sigma(I)]	R1 = 0.0423, wR2 = 0.1017
R indices (all data)	R1 = 0.0468, wR2 = 0.1042
Twin Component Ratio	0.55(5)/0.45(5)
Largest diff. peak and hole	1.466 and -1.614 e.Å^{-3}

Table S6. Bond lengths [Å] and angles [°] for (**4**).

Pd-O(1)	2.005(3)	C(7)-C(8)	1.383(8)
Pd-O(3)	2.017(4)	C(8)-C(9)	1.384(8)
Pd-N(2)	2.020(5)	C(9)-C(10)	1.382(8)
Pd-N(1)	2.023(5)	C(11)-C(12)	1.518(7)
O(1)-C(11)	1.288(6)	C(12)-C(13)	1.378(7)
O(2)-C(11)	1.234(6)	C(12)-C(17)	1.409(7)
O(3)-C(18)	1.301(6)	C(13)-C(14)	1.381(7)
O(4)-C(18)	1.241(6)	C(14)-C(15)	1.388(7)
N(1)-C(1)	1.347(7)	C(15)-C(16)	1.393(7)
N(1)-C(5)	1.353(6)	C(16)-C(17)	1.376(7)
N(2)-C(10)	1.343(6)	C(18)-C(19)	1.486(7)
N(2)-C(6)	1.361(6)	C(19)-C(20)	1.396(7)
C(1)-C(2)	1.383(8)	C(19)-C(24)	1.406(6)
C(2)-C(3)	1.382(7)	C(20)-C(21)	1.375(7)
C(3)-C(4)	1.381(7)	C(21)-C(22)	1.392(7)
C(4)-C(5)	1.369(8)	C(22)-C(23)	1.383(7)
C(6)-C(7)	1.376(8)	C(23)-C(24)	1.380(7)

O(1)-Pd-O(3)	176.77(19)	O(2)-C(11)-O(1)	125.1(5)
O(1)-Pd-N(2)	91.20(16)	O(2)-C(11)-C(12)	119.5(4)
O(3)-Pd-N(2)	91.89(16)	O(1)-C(11)-C(12)	115.4(4)
O(1)-Pd-N(1)	89.69(16)	C(13)-C(12)-C(17)	119.5(4)
O(3)-Pd-N(1)	87.21(16)	C(13)-C(12)-C(11)	120.0(4)
N(2)-Pd-N(1)	178.91(18)	C(17)-C(12)-C(11)	120.4(4)
C(11)-O(1)-Pd	116.4(3)	C(12)-C(13)-C(14)	120.8(5)
C(18)-O(3)-Pd	113.9(3)	C(13)-C(14)-C(15)	119.8(5)
C(1)-N(1)-C(5)	119.2(5)	C(14)-C(15)-C(16)	119.8(4)
C(1)-N(1)-Pd	120.5(3)	C(17)-C(16)-C(15)	120.4(4)
C(5)-N(1)-Pd	120.2(3)	C(16)-C(17)-C(12)	119.5(4)
C(10)-N(2)-C(6)	117.7(4)	O(4)-C(18)-O(3)	123.9(5)
C(10)-N(2)-Pd	120.6(3)	O(4)-C(18)-C(19)	120.3(4)
C(6)-N(2)-Pd	121.7(3)	O(3)-C(18)-C(19)	115.8(4)
N(1)-C(1)-C(2)	121.2(5)	C(20)-C(19)-C(24)	118.2(4)
C(3)-C(2)-C(1)	119.9(5)	C(20)-C(19)-C(18)	119.7(4)
C(4)-C(3)-C(2)	117.9(6)	C(24)-C(19)-C(18)	122.0(4)
C(5)-C(4)-C(3)	120.5(5)	C(21)-C(20)-C(19)	121.4(5)
N(1)-C(5)-C(4)	121.2(5)	C(20)-C(21)-C(22)	119.9(5)
N(2)-C(6)-C(7)	122.3(5)	C(23)-C(22)-C(21)	119.5(5)
C(6)-C(7)-C(8)	119.5(5)	C(24)-C(23)-C(22)	120.9(5)
C(7)-C(8)-C(9)	118.5(5)	C(23)-C(24)-C(19)	120.1(4)
C(10)-C(9)-C(8)	119.3(5)		
N(2)-C(10)-C(9)	122.7(5)		

[1] Steinhoff, B. A.; Stahl, S. S. *Org. Lett.* **2002**, *4*, 4179-4181.

[2] Bruker-AXS. (2000-2001) SADABS V.2.03, SAINT V.6.22, SHELXTL V.6.10 & SMART 5.622 Software Reference Manuals. Bruker-AXS, Madison, Wisconsin, USA.